ISSN 0016-7932, Geomagnetism and Aeronomy, 2015, Vol. 55, No. 1, pp. 108–117. © Pleiades Publishing, Ltd., 2015.
Original Russian Text © Yu.V. Yasyukevich, V.I. Zakharov, V.E. Kunitsyn, S.V. Voeikov, 2015, published in Geomagnetizm i Aeronomiya, 2015, Vol. 55, No. 1, pp. 113–122.

The Response of the Ionosphere to the Earthquake in Japan on March 11, 2011 as Estimated by Different GPS-Based Methods

Yu. V. Yasyukevich[a, c], V. I. Zakharov[b], V. E. Kunitsyn[b], and S. V. Voeikov[a]

[a] *Institute of Solar-Terrestrial Physics, Siberian Branch, Russian Academy of Sciences, ul. Lermontova 126a, Irkutsk, 664033 Russia*

e-mail: yasyukevich@iszf.irk.ru

[b] *Faculty of Physics M.V.Lomonosov Moscow State University, Leninskie Gory, Moscow, 119991 Russia*

[c] *Irkutsk State University, Faculty of Physics, bul'v. Gagarina 20, Irkutsk, 664003 Russia*

Received January 27, 2014; in final form, May 21, 2014

Abstract—The results of detecting ionospheric disturbances by different methods based on GPS observations during the mega-earthquake in Japan (March 11, 2011) are analyzed. It is shown that different methods of analysis and data processing technologies provide generally similar results and suggest quite a complex morphology of the ionospheric response to this seismic event. We distinguish three types of wave disturbances that appeared in the ionosphere in response to the earthquake: slow gravity waves, acoustic–gravity oscillations, and fast disturbances corresponding to the Rayleigh waves. Such an analysis of the wave phenomena and the comparison between the results provided by different methods has been carried out for the first time.

DOI: 10.1134/S0016793214060218

1. INTRODUCTION

The mega-earthquake in Japan occurred on March 11, 2011 at 0546:24 UT. Its magnitude was $Mw = 9.0$ and the epicenter was located at 38.322° N, 142.369° E. The significant power of this event attracted the strong interest of geophysicists (Gokhberg et al., 2011; Astafyeva et al., 2011; Liu et al., 2011; Rolland et al., 2011; Tsugawa et al., 2011) as favorable for gaining more detailed insight into the interactions between different geospheres. The main shock of this temblor was preceded by a few foreshocks having lower magnitudes ($Mw > 6.0$). The main shock was followed by strong aftershock activity, which included 60 quakes with $Mw > 6.0$ and three quakes with $Mw > 7.0$. The rupture originated at a depth of about 24.4 km (www.iris.edu/news/events/japan2011). According to the estimates, the length of the rupture was 380–400 km and the field of the aftershocks covered about 450 km. It was calculated that the earthquake was a low-angle thrust event on a gently dipping fault plane (http://www.tectonics.caltech.edu/slip_history/2011_tohoku-oki-tele/index.html; www.gsi.go.jp/cais/topic110422-index-e.html) and the amplitude of the thrust was 25–30 m; moreover, an analysis involving the entire complex of the data upgraded this value to 35 m (Yokota et al., 2011). The block of the islands of Japan has moved eastwards relative to the Pacific Plate in a direction that is nearly perpendicular to the plate contact. In Figs. 1a and 1 b, this region is shown by the thick black line.

For analyzing the responses of the ionosphere to different geophysical events, it is quite common to use estimates of the total electron content (TEC) I derived from the dual-frequency phase measurements of GPS signal (Hofmann-Wellenhof, 1998):

$$I = \frac{1}{40.308}\frac{f_1^2 f_2^2}{f_1^2 - f_2^2}\left[\left(L_1\lambda_1 - L_2\lambda_2\right) + K + nL\right], \quad (1)$$

where f_1 and f_2 are carrier frequencies of GPS signals; $L_1\lambda_1$, $L_2\lambda_2$ are the additional paths of radio signals due to the phase delay in the ionosphere, m; L_1 and L_2 are the numbers of the full cycles of GPS carrier phases λ_1 and λ_2 are the wavelengths, m; K is a constant due to the phase ambiguity and mistiming between the frequency channels; and nL are the phase-path errors.

Applied to data from the GEONET network (Japan), which includes ~1200 stations, this method provides sufficiently high spatial resolution. The time resolution of the free-access data is 30 s.

2. SPATIAL STRUCTURE OF THE WAVE DISTURBANCES IN TEC BASED ON MAPPING THE TEC VARIATIONS

Saito et al. (1998) suggested the algorithm for visualizing the spatial distribution (mapping) of the intensity of TEC variations reflecting the irregular structure of the ionosphere, which is based on the use of data from dense networks of GPS receivers, such as the GPS receiving networks in Japan and California. For

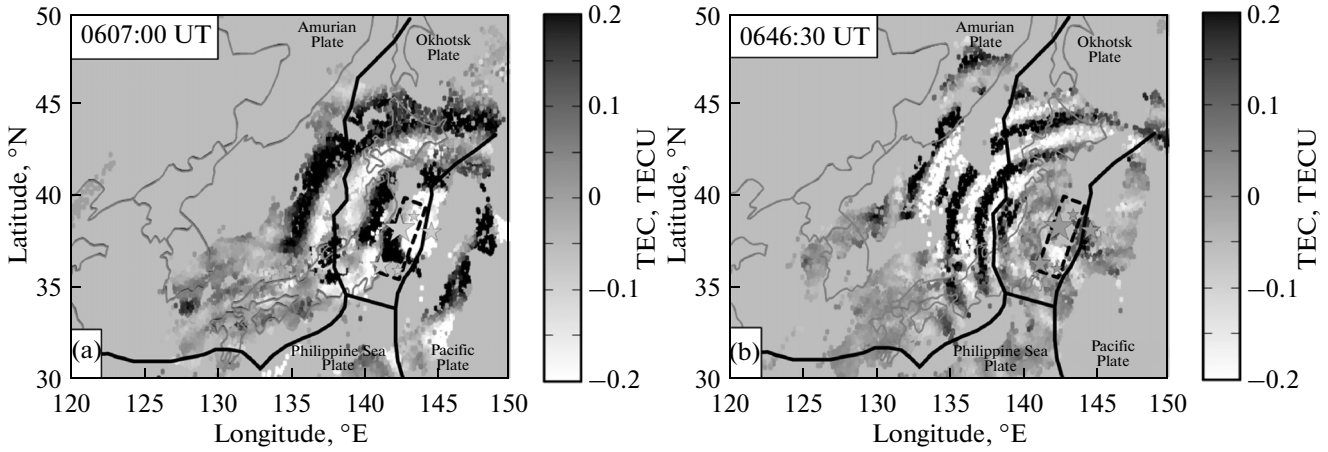

Fig. 1. Spatial distribution of TEC variations according to the data from all GPS satellites at (a) 0607:00 UT and (b) 0646:30 UT on March 11, 2011. The box shown by the dashed line indicates the area of maximal crustal displacements during the earthquake; the asterisks mark the epicenters of the main shock and strongest aftershocks; the thick black line shows the plate contact.

each current time instant, the positions of the subionospheric points (ionospheric piercing points, IPP) are plotted as colored dots, the color of which corresponds to the current amplitude of TEC variations on a given receiver-to-satellite path.

Initially, the time series of the slant TEC were converted to the equivalent vertical TEC in order to normalize the amplitude of the perturbation. This conversion is typically carried out according to the formula of (Klobuchar, 1986), which is obtained with the approximation of a spherically symmetric ionosphere:

$$I_V = I_S \cos\left[\arcsin\left(\frac{R_E}{R_E + h_{\max}}\cos\theta_s\right)\right], \qquad (2)$$

where R_E is the Earth's radius, $h_{\max}$ is the ionospheric $F2$ peak height; θ_s is the elevation angle of the navigation satellite (the angle between the line of sight and the Earth's surface).

After this, the data were filtered by the method of moving average within a window of 2–10 min. The TEC maps demonstrate rather complex interference pattern with two types of TEC perturbations, which are structurally close to the ring waves diverging from the epicenter. The examples of these perturbations are presented in Figs. 1a and 1b. In the interval from 0550 to 0625 UT, we see fast moving large-scale (LS) perturbations with the wavelength $\lambda \approx 600$ km (Fig. 1a). After 0617 UT, the maps show the presence of the medium-scale (MS) perturbations with $\lambda \approx 200$ km (Fig. 1b), which propagate significantly slower than the LS perturbations. The highest intensities of IS perturbations are observed off the epicenter in the northwestern segment of the region.

The estimate of the center of the perturbation under the assumption of a ring shape of the perturbation indicates that the apparent ionospheric source is somewhat shifted off the zone of the earthquake and is located at 37° N, 145° E, which is close to the estimated position of the ionospheric source in (Tsugawa et al., 2011).

From 0556 to 0559 UT, the reconstructions reveal an intense fast LS perturbation. The dynamics of propagation of this structure is illustrated in Fig. 2. This perturbation was moving to the southwest, more or less parallel to the plate contact. As the perturbation moved further away from the epicenter, its intensity rather rapidly decreased. The less intense and faster perturbations propagating in the southwest direction were observed south of the epicentral area up to 0700 UT.

Significantly later after the main shocks of the earthquake, the southeastern part of Japan was in the area of turbulized ionosphere, which was marked with a highly heterogeneous spatial structure of TEC variations (indicated by the oval in Fig. 3). This area slowly drifted to the north and existed from 0800 to 0945 UT. It again appeared after 1030 and persisted up to 12 UT.

3. DISTANCE–TIME DIAGRAMS

It has recently become quite a widespread practice to estimate the velocity of the ionospheric perturbations with the use of the distance–time diagrams suggested in (Calais et al., 2003). The idea of this approach is to correlate the intensity of TEC variations to the time and distance to the source of the ionospheric perturbations (epicenter of the earthquake). The resulting time series of TEC are filtered in the selected interval of periods, after which the satellite elevations, line-of-sight azimuths, and coordinates of IPPs are computed for each time instant and each measurement based on the data on the positions of the satellite. For each IPP, the great-circle distance to the selected source of the perturbations is computed. This yields a two-dimensional (2D) map of TEC variations in the distance–time coordinates, where the color (or

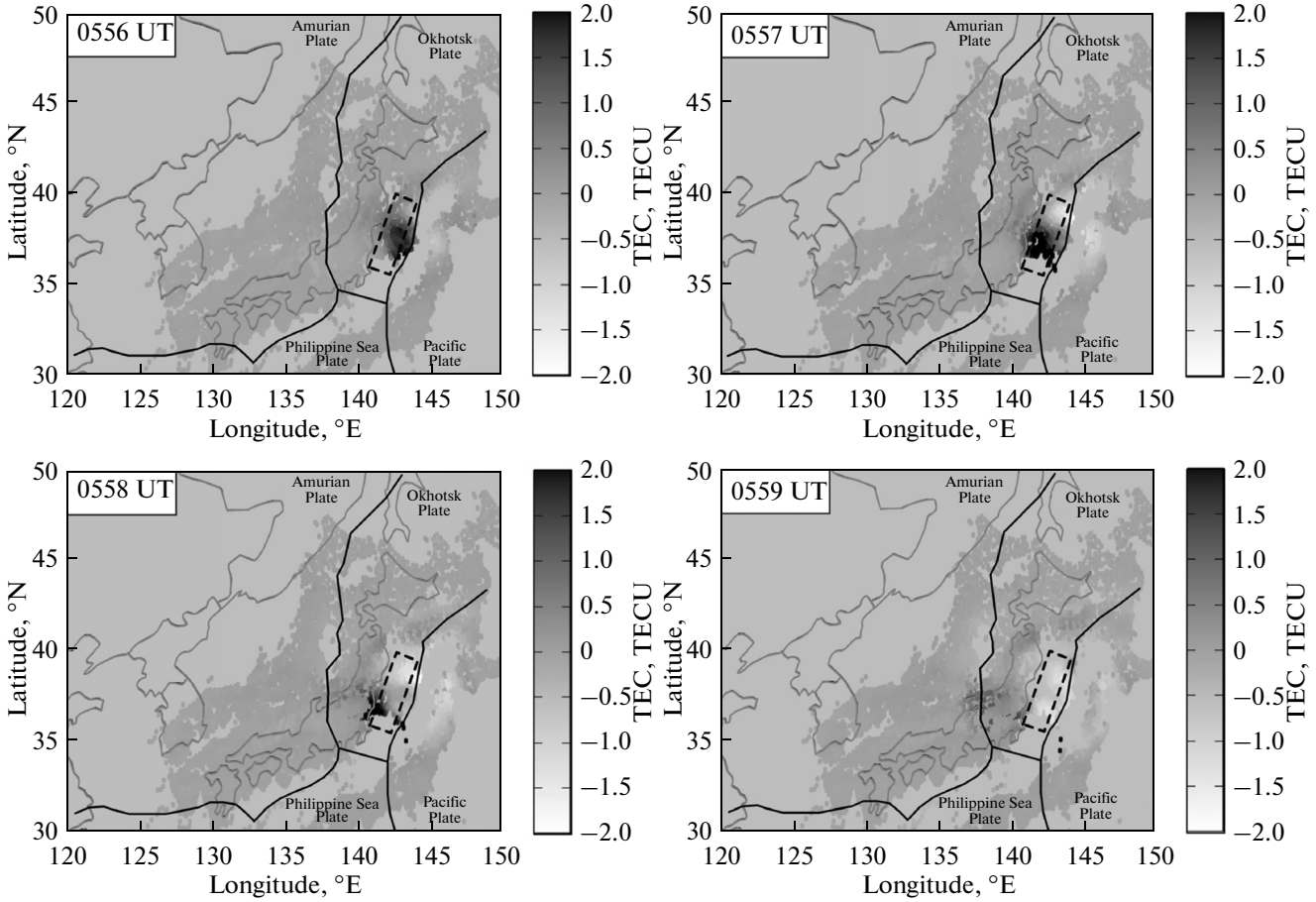

Fig. 2. Dynamics of the spatial distribution of TEC variations at 0556–0559 UT on March 11, 2011. The box shown by the dashed line indicates the area of maximal crustal displacements during the earthquake; the thick black line shows the plate contact.

intensity of monochrome scale) of a point characterizes the intensity of TEC variations.

Within the spherical wave approximation, the maximum of the perturbation will be linearly migrating in the course of time along the radius vector, which will produce the line in the distance–time diagram, the slope of which reflects the propagation velocity of the perturbation. Moreover, this method is capable of identifying different modes contained in the perturbation that move with different velocities.

Figure 4 shows the distance–time diagrams constructed for the (a) northwestern and (b) southern regions of the earthquake. We also analyzed the perturbations southwest and northeast of the earthquake. The vertical gray line shows the time of the Tohoku main shock. The diagrams quite clearly show three modes of perturbation: fast mode, with a velocity of 2.2–2.6 km/s; intermediate mode, with 700–1000 m/s; and slow mode, with 150–300 m/s. The velocities of each mode in the different segments of the region are rather similar (the difference is at most 15–20%).

It is probable that the fast mode of the perturbation, which moves at 2.2–2.6 km/s, is associated with the propagation of the Rayleigh surface wave (Kunitsyn et al., 2011; Tsugawa et al., 2011). For fast mode, the highest amplitude, which is estimated from the positive crest of the perturbation, is observed in the central part of Japan, slightly southward of the epicenter of the earthquake, where it measures ~1.3 TECU (Fig. 4b). The intensity of this mode in the southwestern direction is ~0.2 TECU. In the northwestern azimuth, this mode is less intense (~0.1 TECU, Fig. 4b) and can only be distinguished with a higher contrast of imaging. In the northwestern bearings, fast mode is indistinguishable against natural fluctuations. Highly intense fast mode is only observed in the central regions of Japan, south of the epicenter and close to the area of maximal slip in the seismic source. In other words, the majority of fast mode energy propagates from the epicenter along the fault trend. The propagation azimuth of the fast mode coincides with the direction of the plate contact.

The velocity of the intermediate mode (700–1000 m/s) is commensurate with the speed of sound at the iono-

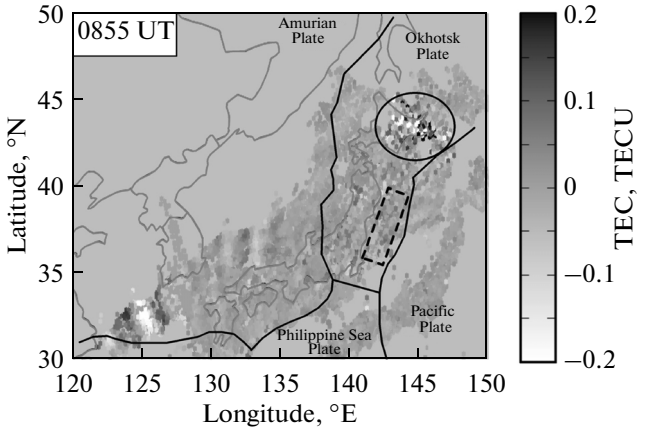

Fig. 3. Spatial distribution of TEC variations at 0855 UT on March 11, 2011. The box shown by the dashed line indicates the area of maximal crustal displacements during the earthquake; the thick black line shows the plate contact.

spheric heights. The amplitude of TEC variations for the intermediate mode is about 0.35 and 0.5 TECU for the southward and northward propagation azimuths, respectively. Kunitsyn et al. (2011) and Tsugawa et al. (2011) associate this mode with the acoustic waves generated in the epicenter of the earthquake.

Besides these modes, the perturbations propagating with the velocities of 150 to 300 m/s are also quite clearly observed in the diagrams. These velocities are close to the sound velocities in the lower atmosphere. The spatial distribution of this mode (see section 1) indicates that the wavelength of this perturbation is ~200 km. Tsugawa et al. (2011) conjecture that this perturbation is caused by the gravity mode of atmospheric waves generated by the earthquake. In this case, the perturbation with a velocity of ~150 m/s is not observed in all directions. The wave that propagates at ~300 m/s has the amplitude of ~1.3 TECU in the northwestward direction, ~0.4 TECU in the northeastern direction, and ~0.6 in the southwester direction. In other words, the gravity branch of the disturbances has a higher intensity in the northwestern azimuths.

4. ANALYSIS OF THE PROPAGATION VELOCITY OF THE MEDIUM- AND LARGE-SCALE PERTURBATIONS BY THE SADM-GPS METHOD

Afraimovich et al. (1997) developed and efficiently tested the GPS-based statistical angle-of-arrival and Doppler method (SADM-GPS) for analyzing the dynamics of the travelling ionospheric disturbances (TIDs) revealed by transionospheric probing. The method is based on measuring the derivatives of TEC with respect to time $I'_t(t)$ and spatial coordinates $I'_y(t)$, $I'_x(t)$ at three receiving sites. This set of the three points is a GPS array with a minimal necessary set of elements sufficient for estimating the velocity and direction of propagation of the ionospheric perturbation. In this case, the distances between points (the length of the base of the array) should be less than half the expected wavelength λ of the perturbation. The GPS satellite velocity is commensurate with the phase velocity of TIDs, and in this case the satellite motion should be necessarily taken into account.

The method relies on a simple model of migration of the phase interference pattern, which moves without changing its shape. The allowance for satellite motion consists of introducing the IPP velocity (which is estimated from the time series of the satellite elevations $\theta_s(t)$ and azimuths $\alpha_s(t)$) into the calculations. The distances between the elements of the array are significantly smaller than the satellite orbital height (>20000 km); therefore, the geometry of the array at

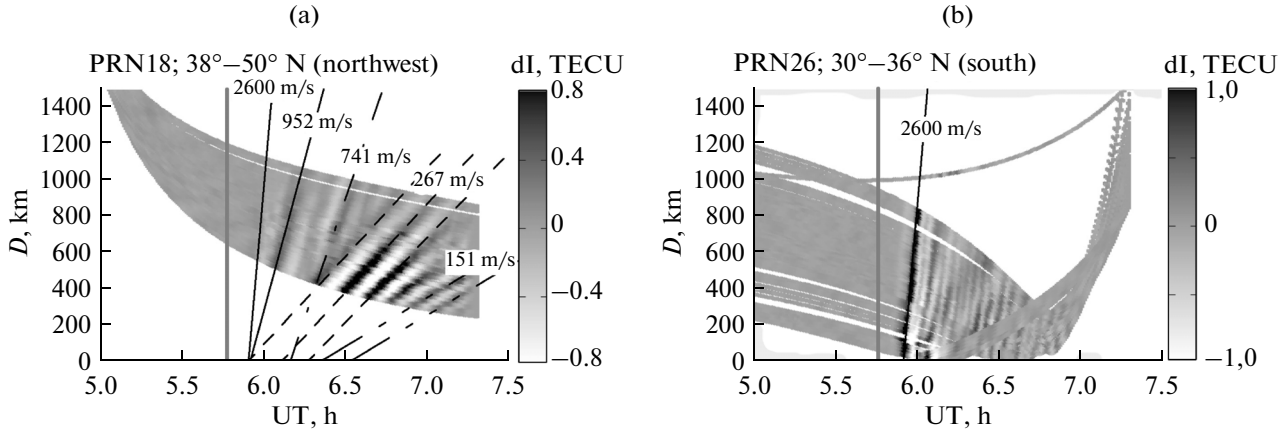

Fig. 4. Distance–time diagrams according to (a) GPS PRN18 and (b) GPS PRN26 satellites for the northwestern and southern parts of the earthquake area.

height h_{max} and on the Earth's surface differ insignificantly, and, hence, it can be assumed that the motion of IPPs occurs in one plane. The horizontal velocity $V_h(t)$ and the azimuth $\alpha(t)$ of the perturbation are determined in the following way (Afraimovich and Perevalova, 2006):

$$\alpha(t) = \arctan(I'_x(t)/I'_y(t)),$$

$$u_x(t) = I'_t(t)/I'_x(t) = u(t)/\sin\alpha(t),$$

$$u_y(t) = I'_t(t)/I'_y(t) = u(t)/\cos\alpha(t),$$

$$u(t) = |u_x(t)\, u_y(t)|(u_x^2(t) + u_y^2(t))^{-1/2},$$

$$V_h = u(t) + w_x(t)\sin\alpha(t) + w_y(t)\cos\alpha(t),$$

where $u(t)$ is the horizontal velocity of the perturbation and $w_x(t)$ and $w_y(t)$ are the velocity components of IPP in the fixed (immobile) coordinate system.

With the dense GPS receiving network in Japan, it is possible to obtain a sufficient number of arrays that obey the constraints on the base length and geometry of the array. The length of the base was selected in an interval from 10 to 25 km in order to satisfy the condition that half the wavelength be less than half the length of the base.

Figure 5 shows the distributions of azimuthal deviations of the perturbation $P(\Delta\alpha)$ from radial propagation as well as the velocities $P(V)$ for the (a) MS and (b) LS perturbations estimated by the SADM-GPS technique for the set of the arrays based on the data from all satellites (the gray filled triangles) and the PRN18 satellite (the black empty boxes). For constructing the distribution, for two time intervals when large-scale perturbations (0552:30–0625:30 UT) and only medium-scale perturbations (0625–0717 UT) were observed, we selected the arrays and calculated the horizontal velocity $V_h(t)$ and azimuth $\alpha(t)$ of the perturbation by formulas (3). Then, for each array, we computed the average values of the velocities and azimuths and determined the azimuth of radial propagation of the perturbation α_r from the source of the perturbation (37° N, 145° E for MS perturbations and the epicenter of the earthquake for the LS perturbations) to the central station of the array. Based on these values, we constructed the distributions of the velocity $P(V)$ and deviations of the azimuths from radial propagation $P(\Delta\alpha)$. The histogram bins were selected to be 10° for the azimuthal deviations and 25 m/s for the velocity.

The SADM-GPS method has certain limitations. Although it provides sufficiently good estimates of the azimuths of perturbations, the velocity estimates have significant scatter (Afraimovich, 1997). Moreover, the situation is complicated in soundings with the use of the satellite systems by the so-called aspect (or geometrical) effect, i.e. the dependence of the amplitude of recorded TEC on the geometry of sounding (Afraimovich and Perevalova, 2006). Because of this, TEC variations turn out to be selective, i.e. they are most sensitive to the perturbations that move perpendicular to the receiver-to-satellite ray. Therefore, it is preferable in some cases to analyze the data from a separate satellite. According to the spatial distribution of TEC variations, it is reasonable to use the PRN18 satellite for analyzing the LS perturbations alone on the time intervals indicated above. Because of the significantly longer lifetime of the MS structures, the parameters of these perturbations are sufficiently well determined from all satellites.

In accordance with the selected 10° bin of the azimuthal deviation histograms, we can only determine the interval of the most probable values. The most probable deviations of the propagation of MS perturbations from the radial lie in the interval from 0° to 10°, and in the case of LS perturbations the most probable azimuthal deviations are –20° to –10° (according to the data from all satellites). The distribution of the azimuthal deviations $P(\Delta\alpha)$ for LS perturbations estimated from PRN18 has high dispersion, with the most probable values lying within 20° to 30°.

The distributions of both the (d) velocities and (b) azimuthal deviations for MS perturbations are quite narrow. The propagation of the LS and MS perturbations is predominantly radial; however, in the case of LS waves, there is a large scatter in the values. According to the PRN18 data, the average horizontal velocity of MS perturbations is $V_h = 250 \pm 50$ m/s (with the most probable value in the interval of 225 to 250 m/s), and the velocity of LS perturbations is $V_h = 590 \pm 200$ m/s (with the most probable value of 625 to 650 m/s). According to the data from all satellites, $V_h = 260 \pm 80$ m/s for the MS perturbations (the most probable velocity is 225–250 m/s) and $V_h = 520 \pm 260$ m/s in the case of LS (the most probable velocity is 425–450 m/s). The lower velocity of LS perturbations estimated from all satellites is due to the fact that part of the satellites recorded MS perturbations, which are slower, during the observation interval.

5. CLUSTER ANALYSIS OF THE DATA PROVIDED BY GPS INTERFEROMETRY

Different methods have been widely developed recently in geophysics for spatiotemporal classification of the observed structures. Among these methods is cluster analysis, which is used as a means for clustering the objects identified by primary analysis into groups described by similar parameters (Gvishiani and Dubois, 2002; Zakharov and Budnikov, 2012).

In this work, we identified irregularities with certain similar characteristics by applying the cluster classification. They were detected by different cells of GPS network using the modified SADM-GPS method. The basic method described in (Afraimovich and Perevalova, 2006) was complemented with a technique which, alongside TEC, also uses the $L1$ phase

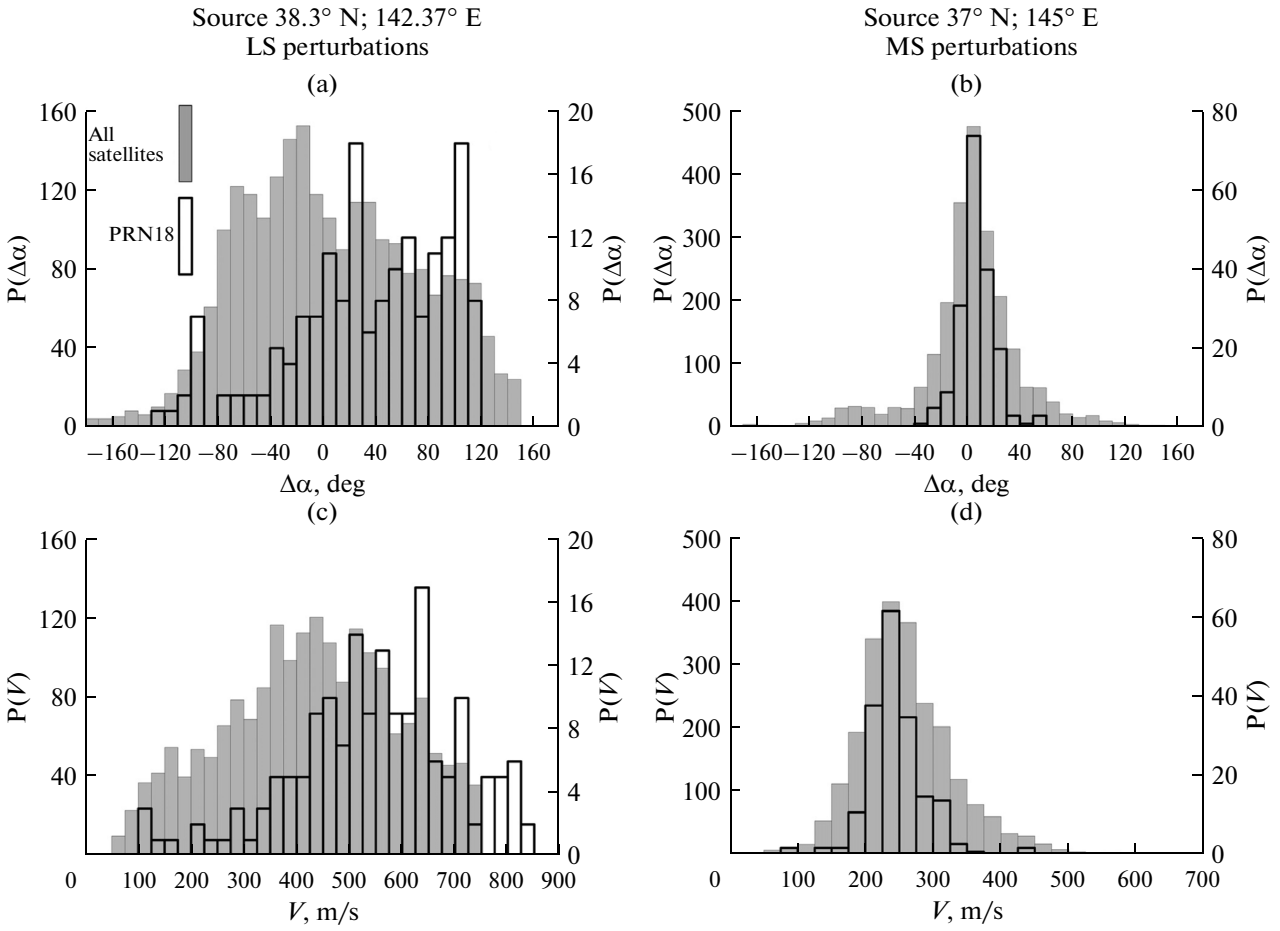

Fig. 5. Distributions of the (c, d) velocities and (a, b) deviations of the azimuths from the radial propagation for the (a, c) LS and (b, d) MS perturbations. The gray boxes correspond to the results based on the data from all satellites; the black line shows results based on the GPS PRN18 data.

variations data for expanding the statistics of the estimates (Zakharov and Zienko, 2007; Zakharov et al., 2008). The cluster analysis was based on four parameters. Two parameters are the geodetic coordinates, the third parameter is the direction of motion of the irregular structure, and the fourth parameter is the time of observation of the structure by cells of the network (Zakharov and Budnikov, 2012). The CRASS-GPS software package, designed at the Faculty of Physics of the Moscow State University, implements a complex algorithm based on the modified method of *k*-averages. Analysis of the results of clustering applied to the data of GPS interferometry shows (Zakharov and Budnikov, 2012) that this approach provides efficient multidimensional data filtering and, as a result, yields stable estimates of the parameters of a particular cluster structure.

Analysis of the relative number of LS wave structures grouped into clusters (a proxy for wave activity) in the period from 7 to 14 March 2011 reveals a local maximum on March 11 at 00–06 UT, which corresponds to the direct response of the ionosphere on the main shock itself (Fig. 6). Here, the LS structures are understood as spatial wave formations with a size of at least 500 km and characteristic periods of at least 15 min.

Figure 6 shows the normalized probability of occurrence of LS wave structures normalized to the maximum value. During the time interval around the earthquake, the occurrence frequency of these structures reached 50% after a relative lull on March 9–10, when the activity did not even achieve the level of 10% in excess of the sensitivity threshold of the method to the occurrence of LS structures. It is remarkable that we revealed the growth and global (on the interval of our analysis) maximum of the LS wave activity on the subsequent days (March 12 and 13). This fact is likely to be associated with aftershock activity and additional turbulization of the upper atmosphere by the series of weaker earthquakes mentioned above.

For the day of the temblor, we carried out additional analysis of the GPS interferometry data. Because of the significant volume, the calculations were only conducted for the data from 96 observation

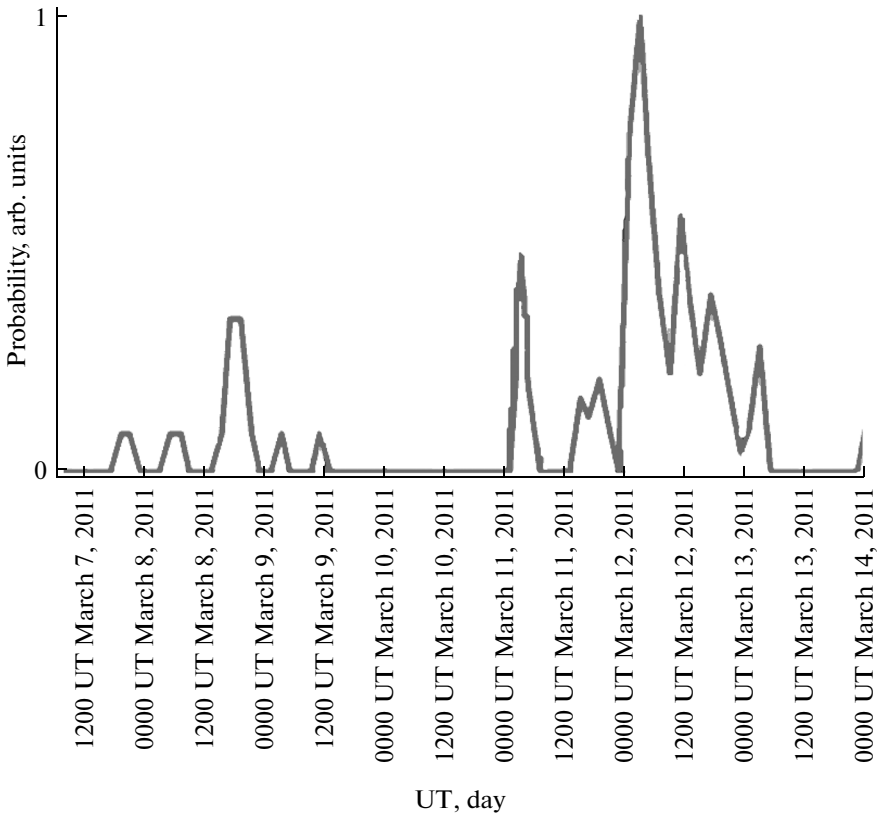

Fig. 6. Wave activity (the probability of occurrence of LS wave structures) in Japan from March 7 to March 14, 2011.

cells that are maximally widely spaced out over the territory of Japan. In this analysis, we used all of the GPS satellites that were simultaneously visible by the cells. The clustering revealed a few LS structures that are coupled in time and probably describe the front of the quasi-ring wave diverging from the source. The IPP of these structures fall within a circle with a radius of 5° around the source (earthquake) and, generally, may reflect both the acoustic perturbation and the ionospheric disturbances induced by the Rayleigh wave (Fig. 7). Based on this data, the average (over the sectors) velocity of the fast mode diverging directly from the epicenter is estimated at $V_h = 2040 \pm 580$ m/s. The sector-average velocities of the wave structure for separate sectors are presented in Table 1. The average velocity in a given sector is denoted by $\langle V \rangle$ with a variance (dispersion) σ_V. The Table also includes the average azimuths of motion for the separate parts of the wavefront of the structure and the variance (dispersion) of these azimuths. The quite high (nearly 30%) relative error of the velocity estimate is due to the fact that we used for identifying this wave a time series with a length of 1 h instead of the normally used 2-hour data. This was done because of the high velocity of this structure, which only comes outside the field of view of the observation networks during a time interval longer than 1 h.

Table 1. Estimates of the parameters of the spherical diverging wave identified during the interval of 0530–0630 UT on March 11, 2011

Sector	$\langle V \rangle$, m/s	σ_V, m/s	$\langle Az \rangle$, deg	σ_{Az}, deg
1	2660	400	330	20
2	2200	520	200	22
3	1370	440	270	29
4	1870	640	45	29
5	2080	900	290	24

We note the high velocities of the identified fragments of the wave front in sectors 1 and 2, which correspond to the time of the direct response to the earthquake. It is remarkable that the velocities in these sectors correspond to the velocity of the Rayleigh surface wave (Brekhovskikh, 1973). One identified component travels along the plate boundary that is located in the vicinity of the epicenter of the earthquake, and the other propagates almost perpendicular to this boundary (Fig. 1).

The perturbations identified in sectors 3 and 4 are probably associated with the propagation of the acous-

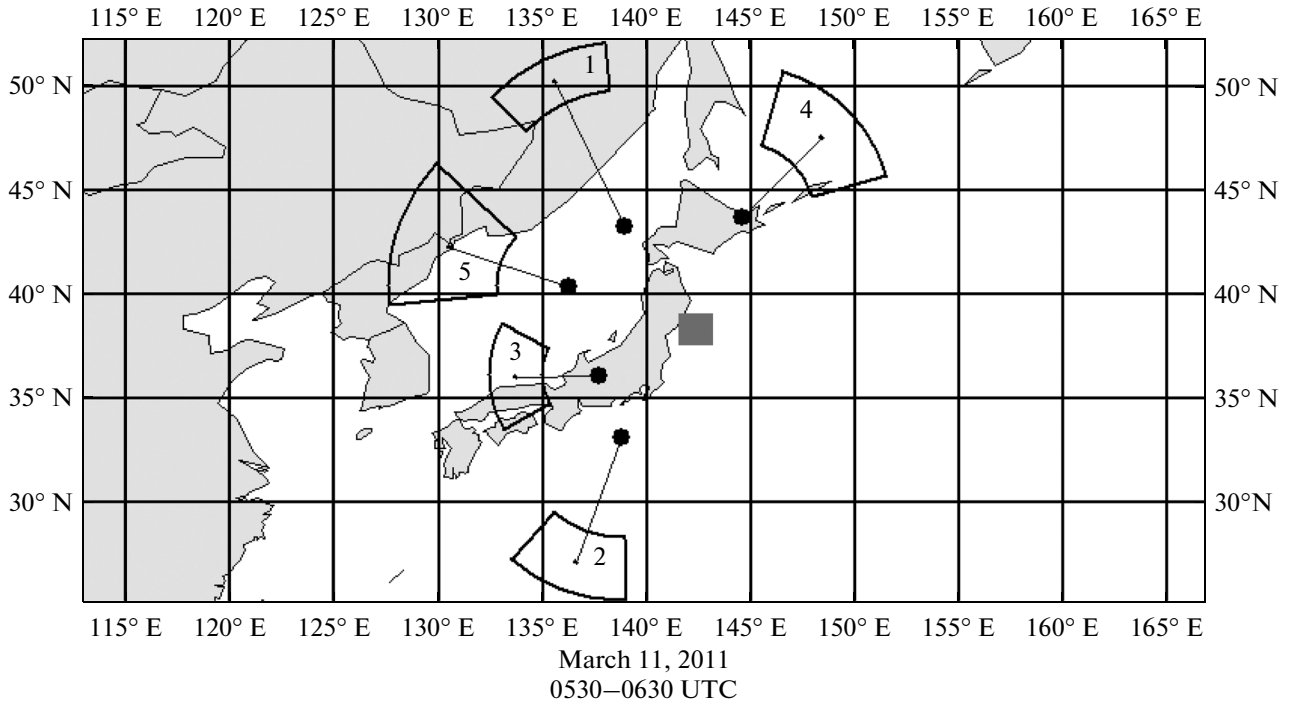

Fig. 7. Positions of IPPs of the wave structure revealed by the cluster analysis. The box shows the epicenter of the main shock.

tic mode of the perturbation. The high velocities and errors of identification of the revealed structures may also be due to the interference of the waves recognized by the analysis in Section 2 that form a spherical front. For example, we tend to interpret the segment of the wavefront shown in sector 5 as resulting from this interference.

Our analysis demonstrates the complex character and probable mutual influence of the coseismic and postseismic ionospheric processes. Cluster analysis identifies the studied ionospheric structures as resulting from the transient process triggered by the pulse impact from the earthquake exactly in the time interval from 0530 to 0630 UT. It is remarkable that the directions of the motion of the ionospheric structures revealed by the cluster analysis agree with the results of other methods; the maximal amplitude of the acoustic mode is revealed in the northwestern azimuth.

6. CONCLUSIONS

For the discussion, we summarize our results in Table 2 and compare the velocities of the perturbations estimated by the different methods (SADM-GPS, distance-time diagrams, and cluster analysis).

The data in Table 2 show that the different GPS-based techniques have their own peculiarities and limitations of applicability. Nevertheless, the parameters of the ionospheric wave structures (primarily, the velocities) estimated by these methods from the same set of the initial data qualitatively agree. The application of different GPS-based techniques provides deeper insight into the generation of wave disturbances, since each method sheds light on specific properties and particular features of the observed wave structure that are obscured in the other techniques.

Different methods of GPS-based analysis detected intense ionospheric perturbations directly from the

Table 2. Comparison of the velocities of different modes estimated by different methods in the period of 0500–0730 UT on March 11, 2011

	SADM-GPS (PRN18)	Distance-time diagram	Cluster analysis
Slow gravity mode	250 ± 50 most probable value is 225–250 m/s	150–300 m/s	Not available
Intermediate acoustic mode	590 ± 200 most probable value is 625–650 m/s	700–1000 m/s	1370 ± 440 m/s
Fast mode due to the Rayleigh wave	Not available	2200–2600 m/s	2200–2660 m/s

main seismic event (the main shock at 0556 UT). These perturbations have different spatial and time scales and concentrically diverge from the epicenter.

After the earthquake, starting from 0800 UT, the ionospheric plasma above Japan became strongly turbulized, with a characteristic strongly heterogeneous spatial structure of TEC variations. This area slowly migrated northwards and persisted for almost 2 h up to 1000 UT.

The distance–time diagrams revealed three modes of the ionospheric perturbations from the earthquake: the fast mode, moving with a velocity of 2.2–2.6 km/s; the intermediate mode, with a velocity of 700–1000 m/s; and the slow mode, with a velocity of 150–300 m/s. The velocities of modes in the different propagation sectors differ by 15–20%.

The SADM-GPS method distinguishes two modes: large-scale and medium-scale perturbations with the average horizontal velocities of 635 and 250 m/s, respectively. Both types of the perturbations propagated radially from the epicenter of the earthquake.

Cluster analysis of the SADM-GPS data also revealed the fast mode as corresponding to the response of the ionosphere to the main shock. As a result, based on the obtained data, we identified a few large-scale structures that are coupled in time and can probably describe the front of the ring wave diverging from the epicenter. The propagation velocities of the structures vary from 1.4 to 2.6 km/s, which corresponds to the acoustic and fast-mode perturbations recognized in the distance–time diagrams.

The analysis established significant asymmetry in the propagation of energy of the wave in different azimuths. For the fast mode perturbation, the highest intensity is detected in the southwestern direction parallel to the plate contact; these peak values fall in the vicinity of the area of maximal slip in the source of the earthquake. The slow mode has a higher intensity in the northwestern directions.

Thus, the different methods of analysis and different data processing technologies applied in our study provide generally similar results and suggest a rather complex morphology of the ionospheric response to the Tohoku-oki mega-earthquake. It is remarkable that such a complete analysis of the wave phenomena during an earthquake and the comparison between the results provided by different methods has been carried out for the first time.

Furthermore, the ionospheric response to seismic events is likely to be nonlinear and controlled by a number of factors. For example, analysis of the relative number of occurrences of LS wave structures grouped into the clusters (the wave activity) during the interval from March 7 to 14, 2011 reveals a local maximum from 00 UT to 06 UT on March 11 after a relatively quiet interval on March 9 and 10. This generally agrees with the turbulization of the ionospheric plasma revealed by our study and the response of the ionosphere directly to the main shock. At the same time, further analysis shows an increase in wave activity during the whole day of March 12, with the absolute maximum in the morning hours. This is probably associated with the aftershocks and additional turbulization of the upper atmosphere by a series of weaker temblors that hit the region on March 11 and 12.

ACKNOWLEDGMENTS

We are grateful to N.P. Perevalova for helping with our work. We appreciate the Geospatial Information Authority of Japan (GSI) for providing the data for our analysis. Russian Foundation for Basic Research (grants 12-05-90717-mob_st and 14-05-00855a). Partial support was provided under interdisciplinary integration project 11 of the Siberian Branch of the Russian Academy of Sciences, grant P212-OU-033 under the program for strategic development of the Irkutsk State University for 2012–2014.

REFERENCES

Afraimovich, E.L., Statistical angle-of-arrival and Doppler method (SADM) for determining characteristics of the dynamics of the transionospheric radio signal interference pattern, *Acta Geod. Geophys. Hung.*, 1997, vol. 32, nos. 3–4, pp. 461–468.

Afraimovich, E.L. and Perevalova, N.P., *GPS-monitoring verkhnei atmosfery Zemli* (GPS Monitoring of the Upper Atmosphere of the Earth), Irkutsk: GU NTs RVKh VSNTs SO RAMN, 2006.

Astafyeva, E., Lognonne, P., and Rolland, L., First ionospheric images of the seismic fault slip on the example of the Tohoku-oki earthquake, *Geophys. Res. Lett.*, vol. 38, no. 22, L22104. doi: 10.1029/2011GL049623

Brekhovskikh, L.M., *Volny v sloistykh sredakh* (Waves in Layered Media), Moscow: Nauka, 1973.

Calais, E., Haase, J.S., and Minster, J.B., Detection of ionospheric perturbations using a dense GPS array in Southern California, *Geophys. Res. Lett.*, 2003, vol. 30, no. 12, pp. 1628–1631.

Gokhberg, M.B., Steblov, G.M., Shalimov, S.L., Veic, V.A., and Grekhova, E.A., Ionospheric response to the submarine earthquake in Japan on March 11, 2011 according to GPS satellite observations, *Geofiz. Protsessy Biosfera*, 2011, vol. 10, no. 1, pp. 47–63.

Gvishiani, A. and Dubois, J.O., *Artificial Intelligence and Dynamic Systems for Geophysical Applications*, Berlin: Springer, 2002.

Hofmann-Wellenhof, B., Lichtenegger, H. and Collins, J., *GPS: Theory and Practice*, New York: Springer, 1998.

Klobuchar, J.A., Ionospheric time-delay algorithm for single-frequency GPS users, *IEEE Trans. Aerospace Electron. Syst.*, 1986, vol. 23, no. 3, pp. 325–331.

Kunitsyn, V.E., Nesterov, I.A., and Shalimov, S.L., Japan megathrust earthquake on March 11, 2011: GPS–TEC evidence for ionospheric disturbances, *JETP Lett.*, 2011, vol. 94, no. 8, pp. 616–620.

Liu, J.-Y., Chen, C.H., Lin, C.H., Tsai, H.-F., Chen, C.-H., and Kamogawa, M., Ionospheric disturbances triggered by the 11 March 2011 M9.0 Tohoku earthquake, *J. Geophys. Res.*, 2011, vol. 116, A06319. doi: 10.1029/2011JA016761

Rolland, L.M., Lognonne, P., Astafyeva, E., Kherani, E.A., Kobayashi, N., Mann, M., and Munekane, H., The resonant response of the ionosphere imaged after the 2011 off the Pacific coast of Tohoku earthquake, *Earth Planets Space*, 2011, vol. 63, no. 7, pp. 853–857.

Saito, A., Fukao, S., and Miyazaki, S., High resolution mapping of TEC perturbations with the GSI GPS network over Japan, *Geophys. Res. Lett.*, 1998, vol. 25, no. 16, pp. 3079–3082.

Tsugawa, T., Saito, A., Otsuka, Y., Nishioka, M., Maruyama, T., Kato, H., Nagatsuma, T., and Murata, K.T., Ionospheric disturbances detected by GPS total electron content observation after the 2011 off the Pacific coast of Tohoku earthquake, *Earth Planets Space*, 2011, vol. 63, pp. 875–879.

Yokota, Y., Koketsu, K., Fujii, Y., Satake, K., Sakai, Sh., Shinohara, M., and Kanazawa, T., Joint inversion of strong motion, teleseismic, geodetic, and tsunami datasets for the rupture process of the 2011 Tohoku earthquake, *Geophys. Res. Lett.*, 2011, vol. 38, L00G21. doi: 10.1029/2011GL050098

Zakharov, V.I. and Zienko, A.S., A method for statistical wavelet analysis of ionospheric GPS signals, *Moscow. Univ. Phys. Bull.*, 2007, vol. 62, no. 2, pp. 108–112.

Zakharov, V.I., Zienko, A.S., and Kunitsyn, V.E., The propagation of GPS radio signals at various solar activity, *Elektromag. Volny Elektron. Sist.*, 2008, no. 8, pp. 51–57.

Zakharov, V.I. and Budnikov, P.A., The application of cluster analysis to the processing of GPS interferometry data, *Moscow Univ. Phys. Bull.*, 2012, vol. 67, no. 1, pp. 25–32.

Translated by M. Nazarenko